Optical scanning holography as a technique for high-resolution three-dimensional biological microscopy

Jim Swoger, Manuel Martínez-Corral, Jan Huisken, and Ernst H. K. Stelzer

Light Microscopy Group, European Molecular Biology Laboratory, Postfach 10 22 09, D-69012 Heidelberg, Germany

Received December 3, 2001; revised manuscript received April 11, 2002; accepted April 16, 2002

The applicability of optical scanning holography (OSH) to the field of microscopic imaging for biological applications is assessed. A generalized mathematical description of OSH that takes into account polarization effects, high numerical apertures, and generalized illumination wave fronts is presented. This description is used to show that the proposed single-beam scanning technique relaxes the restrictions under which OSH functions correctly compared with the conventional double-beam scanning method. It is also shown that, although in general OSH is restricted to thin samples, this condition can be relaxed in nonrefracting fluorescence samples, which are of importance in biological microscopy. © 2002 Optical Society of America

OCIS codes: 090.0090, 110.0180, 110.6880, 180.5810, 180.2520, 180.6900.

1. INTRODUCTION

Optical scanning holography (OSH) is a technique that allows three-dimensional (3D) information about an object to be measured with only lateral scanning.[1] The object is illuminated by an interference pattern created by the overlap of two coherent beams, which is scanned across the object. This contrasts with traditional holography, in which a reference beam and an object beam interfere at a detector[2]; this difference is the source of several interesting properties unique to OSH.

One feature of OSH that is not available in traditional holographic techniques is that the light emitted from the object does not need to be coherent. Depending on the system configuration, the hologram can encode either the amplitude or the intensity response of the sample.[3] This allows one to measure, for example, refractive-index variations in a sample that would be practically undetectable with traditional transmission imaging (although these variations could be imaged with traditional holography). Conversely, with OSH one could image in a purely incoherent mode, thus masking phase variations and detecting only the intensity response of the object.

The latter property is of particular interest in the context of the commonly used technique of fluorescence microscopy, as applied to biological problems.[4,5] Traditional holographic microscopy has been used in biology,[6,7] but it is inherently insensitive to incoherent emissions such as fluorescence. Wide-field fluorescence microscopy is a commonly used technique for imaging fluorescence, but for thick samples it requires axial scanning of the sample or the imaging optics. Confocal and multiphoton microscopies[8] can provide high-resolution, optically sectioned, fluorescence images, but these techniques require both axial and lateral scanning. Incoherent OSH therefore can be of use in applications where 3D fluorescence data sets are desired but axial scanning is difficult or impossible.

Although OSH has been demonstrated experimentally[1,9–11] and described theoretically[3,12,13] in the literature, there are some aspects of the technique that merit further consideration. First, although the application of OSH to microscopy has been considered in the literature,[1,3] there are aspects such as polarization effects in high-numerical-aperture (NA) lenses that have not been considered. Second, in much of the previous work,[1,3] one of the beams in the model is assumed to be an ideal uniform plane wave, and consequently the effects of beam aberrations on the reconstructed image are not taken into account. In addition to examining these aspects of OSH, we present the possibility of single-beam scanning, in which only one, rather than both, of the two beams interfering at the sample is scanned. We show that this technique is in general more tolerant of aberrations in the illuminating beams than is the method of scanning both beams.

The purpose of this paper is not to provide detailed simulations of the efficiency or resolving power of particular configurations of OSH (this has been done previously for both Gaussian[13] and truncated-spherical-wave[3] beams). Rather, we provide a general description of the processes involved, with the aim of clarifying which configurations should produce the most useful results, and under which conditions. With the goal of analyzing OSH as a tool for biological microscopy, we consider explicitly the use of high-NA objective lenses.

2. HOLOGRAPHIC PRINCIPLES

A. General Description

In general, the hologram generation process should be describable by the correlation of the sample distribution with an encoding function:

$$H(\mathbf{r}) = f_{\text{sample}}(\mathbf{r}) \otimes f_{\text{enc}}(\mathbf{r}), \tag{1}$$

1084-7529/2002/091910-09$15.00 © 2002 Optical Society of America

where $H(\mathbf{r})$ is the hologram, f_{sample} is the characteristic of the sample that we want to image, f_{enc} is an encoding function, $\mathbf{r}$ is the lateral position vector, and $\otimes$ denotes the correlation of two scalars. In the notation used throughout this paper, vectors are written using boldface, and scalars are in italics. A vector of unit length is denoted by a circumflex, so that we can describe a vector in terms of its length and direction: $\mathbf{a} = a\hat{\mathbf{a}}$.

If Eq. (1) is a valid description of the encoding process, then a reconstructed image of f_{sample} can be generated by

$$I_{\text{rec}}(\mathbf{r}) = H(\mathbf{r}) \otimes R_f(\mathbf{r}), \tag{2}$$

where R_f is the reconstruction function. See, e.g., Klysubun and Indebetouw[14] for an interesting discussion of the applications of various reconstruction functions in spatiotemporal digital holography.

For an ideal, one-to-one reconstruction of the sample, R_f is given by

$$R_{f,\text{ideal}}(\mathbf{r}) = \text{FT}^{-1}[1/\text{FT}(f_{\text{enc}}(\mathbf{r}))], \tag{3}$$

where FT and FT^{-1} denote the Fourier and inverse Fourier transforms, respectively. In this case, the reconstructed image is

$$\begin{aligned} I_{\text{rec}}(\mathbf{r}) &= f_{\text{sample}}(\mathbf{r}) \otimes f_{\text{enc}}(\mathbf{r}) \otimes R_{f,\text{ideal}}(\mathbf{r}) \\ &= f_{\text{sample}}(\mathbf{r}) \otimes \delta(\mathbf{r}) \\ &= f_{\text{sample}}(\mathbf{r}). \end{aligned} \tag{4}$$

Owing to the finite support of $\text{FT}(f_{\text{enc}}(\mathbf{r}))$, in practice Eq. (3) must be modified to avoid division by zero (a familiar problem in inverse filtering applications[15]). In realistic applications, $f_{\text{enc}}(\mathbf{r}) \otimes R_f(\mathbf{r})$ is therefore not a perfect δ function, so the reconstruction, I_{rec}, is not an exact representation of the actual sample, f_{sample}. This represents the fact that any real imaging system has a finite resolution.

A number of different methods for reconstruction are possible: optically, by illuminating a developed photographic plate as in classical holography,[6,16] or with a programmable spatial light modulator,[9,17] or numerically in a computer[18] for digital holography. However, the specific details of these methods are not important for the arguments presented here, which concern only the hologram generation process.

B. Optical Scanning Holography

The process of generating a hologram with the use of OSH has been described in detail in the literature.[1,3] The fundamental process is outlined in Fig. 1, where for simplicity we assume a point object for the sample. This sample is illuminated by a pattern generated by the interference of two beams, which is scanned across the sample. The response of the sample to the illumination (e.g., scattering, fluorescent emission) is detected and recorded as a function of the scan position. Thus, as the illumination pattern is scanned, a signal is produced that is proportional to the illumination intensity at the point object. Although only a one-dimensional line scan is depicted in Fig. 1, in practice a two-dimensional raster scan is used, so the hologram of the point object generated by OSH is simply a map of the illumination pattern. When a Fresnel zone plate is used as the illumination pattern (as depicted in Fig. 1), this yields the same holographic pattern as in traditional on-axis holography.

For a spatially extended sample, the response at the detector is simply the sum of the contributions from each point in the sample. Whether the sum is coherent (the sum is over the amplitude of the signal from each point) or incoherent (sum over intensity) depends on the detector configuration and the nature of the sample's response. Thus the 3D position of each point in the sample is encoded in the location of the center of its Fresnel zone plate (lateral position) and the ring spacing (axial position).

The sample is illuminated by a combination of two coherent beams. With the scanner centered and at rest, (note that we consider only beam scanning here, as opposed to sample scanning, for the hologram generation) the electric-field distribution in the sample region is $\mathbf{E}_o(\mathbf{r})$ for the object beam and $\mathbf{E}_r(\mathbf{r})$ for the reference beam. We assume that the relative phase ϕ between these beams

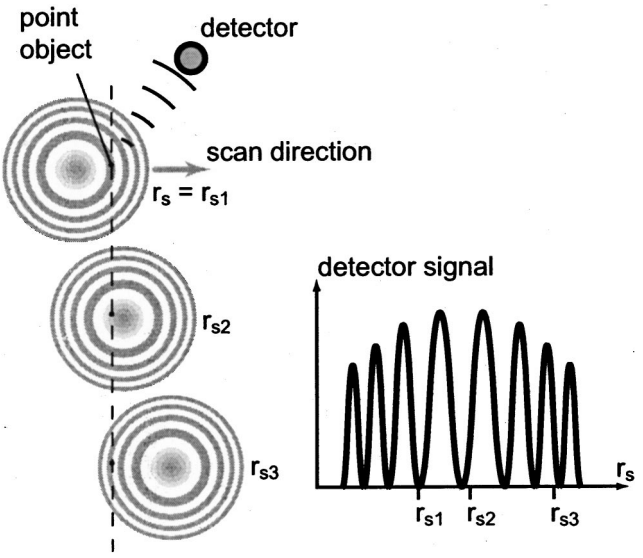

Fig. 1. OSH signal generation. An illumination pattern, created by the interference of coherent beams, is scanned across a point object. The signal at the detector is proportional to the intensity of the illumination pattern at the point object, which varies as the illumination is scanned. The resulting detector signal for a line scan is shown; a 2D raster scan of the point object produces a map of the illumination pattern. For spatially extended objects, the detected signal is the sum of the signals from all of the points in the object.

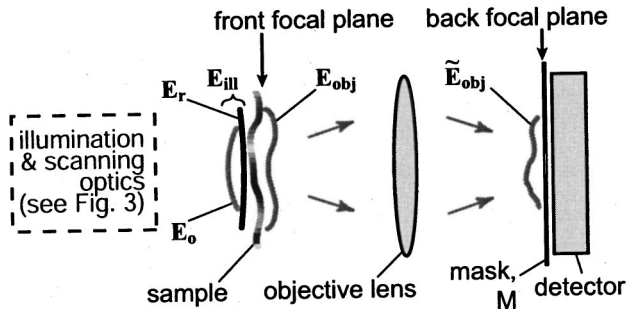

Fig. 2. Important wave fronts in OSH. $\mathbf{E}_o$ and $\mathbf{E}_r$ are incident on the sample; $\mathbf{E}_{\text{obj}}$ exits the sample, and $\tilde{\mathbf{E}}_{\text{obj}}$ is incident on the mask, M. The optics before the sample are not shown.

can be controlled. As can be seen in Fig. 2, the total illumination electric-field distribution just before the sample is then

$$\mathbf{E}_{\mathrm{ill}}(\mathbf{r}) = \mathbf{E}_o(\mathbf{r}) + \exp(i\phi)\mathbf{E}_r(\mathbf{r}). \tag{5}$$

Note that the above description of the illumination is a vectorial one and thus is able to describe high-NA systems in which the polarizations of $\mathbf{E}_o$ and $\mathbf{E}_r$ may be necessarily different.

3. DOUBLE-BEAM SCANNING

We present a generalization of the model for double-beam scanning[3] that accounts for high-NA polarization effects and outlines the conditions under which OSH should be expected to function.

When the illumination pattern is scanned as a unit (i.e., the reference and object beams move together; see Fig. 3), the scanned field is

$$\mathbf{E}_{\mathrm{ill}}(\mathbf{r}, \mathbf{r}_s) = \mathbf{E}_o(\mathbf{r} - \mathbf{r}_s) + \exp(i\phi)\mathbf{E}_r(\mathbf{r} - \mathbf{r}_s), \tag{6}$$

where $\mathbf{r}_s$ is the instantaneous position of the scanned illumination pattern. Just behind the thin object, which has amplitude response T, the electric field is

$$\mathbf{E}_{\mathrm{obj}}(\mathbf{r}, \mathbf{r}_s) = T(\mathbf{r}, t)\mathbf{E}_{\mathrm{ill}}(\mathbf{r}, \mathbf{r}_s). \tag{7}$$

Here we write $T(\mathbf{r}, t)$ explicitly as

$$T(\mathbf{r}, t) = T_{\mathrm{ins}}(\mathbf{r})\exp[i\Psi(\mathbf{r}, t)], \tag{8}$$

where $T_{\mathrm{ins}}(\mathbf{r})$ is the (complex) instantaneous response of the sample at an arbitrary reference time (say, $t = 0$) and $\Psi(\mathbf{r}, t)$ is a phase factor that accounts for the degree of coherence of the response. For a sample with a coherent response, $\Psi(\mathbf{r}, t) = \omega t$; for a purely incoherent sample, $\Psi(\mathbf{r}, t)$ varies randomly with position and time. This construction allows us to make use of the FT relationship between the fields in the front and back focal planes of the objective lens, even when the sample response is incoherent.

In this treatment, the polarization of the detected light is assumed to be the same as that of the illumination [i.e., T_{ins} in Eq. (8) is a scalar, not a tensor]. In the incoherent OSH modes (see Subsections 3.A and 4.A) the signal depends on the total *intensity* at the detector, so the state of polarization of the detected light is irrelevant. In particular, fluorescence (discussed explicitly in Subsection 5.B) is always imaged incoherently because of the random nature of both the polarization and the phase of most samples. For coherent imaging of birefringent samples, the polarization of the detected light may have significant effects on the imaging properties of OSH. However, since this is the case only for a limited range of samples, and for few biological samples in particular, we do not consider this issue in the present paper.

A mask with transmission $M(\boldsymbol{\rho})$ is placed in the back focal plane of the objective lens, where $\boldsymbol{\rho}$ is the position in the back focal plane. If a large-area detector is located behind the mask, the detected intensity signal is given (to within a multiplicative constant) by

$$S(\mathbf{r}_s) = \int\int M(\boldsymbol{\rho})\tilde{\mathbf{E}}_{\mathrm{obj}}(\boldsymbol{\rho}, \mathbf{r}_s) \cdot \tilde{\mathbf{E}}^*_{\mathrm{obj}}(\boldsymbol{\rho}, \mathbf{r}_s)\mathrm{d}^2\boldsymbol{\rho},$$

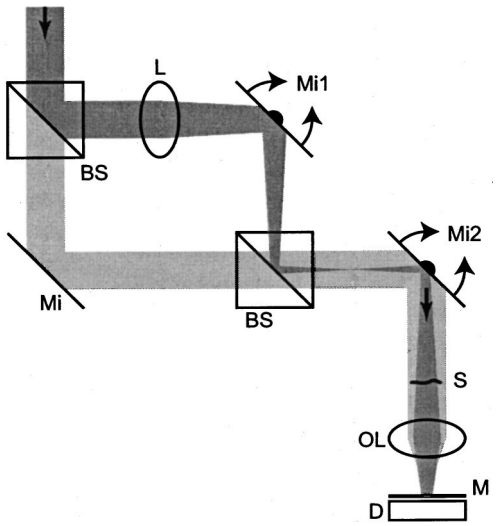

Fig. 3. Schematic of scanning configurations for OSH. For single-beam scanning, Mi1 is used to scan the beam and Mi2 is a fixed mirror. For double-beam scanning, Mi2 is scanned and Mi1 is fixed. The details of the scan optics are not shown. A combination of a plane reference wave and a diverging object wave are shown here; however, the analysis in the text is not restricted to this configuration. BS, beam splitter; L, lens; OL, objective lens; Mi, mirror; S, sample; M, mask; D, detector.

where $\tilde{f}(\boldsymbol{\rho})$ denotes the Fourier transform of $f(\mathbf{r})$ and the asterisk denotes the complex conjugate operation. Note that this formulation assumes that the sample is located in the front focal plane of the objective lens. However, this need not be a restriction in practice, because if $\mathbf{E}_{\mathrm{obj}}(\mathbf{r}, \mathbf{r}_s)$ is known, it can be mathematically forward (or back) propagated to the front focal plane, in which the FT relationship holds. For simplicity, we leave this step implicit in this paper.

Using the FT definition,[19] we have

$$S(\mathbf{r}_s) = \int\int M(\boldsymbol{\rho}) \cdot \left[\int\int \exp(-2\pi i\boldsymbol{\rho} \cdot \mathbf{r}')\mathbf{E}_{\mathrm{obj}}(\mathbf{r}', \mathbf{r}_s)\mathrm{d}^2\mathbf{r}'\right] \cdot \left[\int\int \exp(2\pi i\boldsymbol{\rho} \cdot \mathbf{r}'')\mathbf{E}^*_{\mathrm{obj}}(\mathbf{r}'', \mathbf{r}_s)\mathrm{d}^2\mathbf{r}''\right]\mathrm{d}^2\boldsymbol{\rho}.$$

Rearranging,

$$\begin{aligned} S(\mathbf{r}_s) &= \int\int\int\int \left\{\int\int \exp[-2\pi i\boldsymbol{\rho} \cdot (\mathbf{r}' - \mathbf{r}'')]M(\boldsymbol{\rho})\mathrm{d}^2\boldsymbol{\rho}\right\}\mathbf{E}_{\mathrm{obj}}(\mathbf{r}', \mathbf{r}_s) \cdot \mathbf{E}^*_{\mathrm{obj}}(\mathbf{r}'', \mathbf{r}_s)\mathrm{d}^2\mathbf{r}'\mathrm{d}^2\mathbf{r}'' \\ &= \int\int\int\int \tilde{M}(\mathbf{r}' - \mathbf{r}'')\mathbf{E}_{\mathrm{obj}}(\mathbf{r}', \mathbf{r}_s) \cdot \mathbf{E}^*_{\mathrm{obj}}(\mathbf{r}'', \mathbf{r}_s)\mathrm{d}^2\mathbf{r}'\mathrm{d}^2\mathbf{r}''. \end{aligned}$$

With Eq. (7), which defines $\mathbf{E}_{\mathrm{obj}}$, this becomes

$$S(\mathbf{r}_s) = \int\int\int\int \tilde{M}(\mathbf{r}' - \mathbf{r}'')[T(\mathbf{r}', t)\mathbf{E}_{\mathrm{ill}}(\mathbf{r}', \mathbf{r}_s)] \cdot [T^*(\mathbf{r}'', t)\mathbf{E}^*_{\mathrm{ill}}(\mathbf{r}'', \mathbf{r}_s)]\mathrm{d}^2\mathbf{r}'\mathrm{d}^2\mathbf{r}''. \quad (9)$$

Substituting $\mathbf{E}_{\mathrm{ill}}$, given by Eq. (6), and collecting terms with regard to the phase factor ϕ yields

$$\begin{aligned} S(\mathbf{r}_s) = {} & \int\int\int\int \tilde{M}(\mathbf{r}' - \mathbf{r}'')T(\mathbf{r}', t)T^*(\mathbf{r}'', t) \\ & \cdot [\mathbf{E}_o(\mathbf{r}' - \mathbf{r}_s) \cdot \mathbf{E}^*_o(\mathbf{r}'' - \mathbf{r}_s) \\ & + \mathbf{E}_r(\mathbf{r}' - \mathbf{r}_s) \cdot \mathbf{E}^*_r(\mathbf{r}'' - \mathbf{r}_s)]\mathrm{d}^2\mathbf{r}'\mathrm{d}^2\mathbf{r}'' \\ & + \exp(i\phi)\int\int\int\int \tilde{M}(\mathbf{r}' - \mathbf{r}'') \\ & T(\mathbf{r}', t)T^*(\mathbf{r}'', t)\mathbf{E}_r(\mathbf{r}' - \mathbf{r}_s) \\ & \cdot \mathbf{E}^*_o(\mathbf{r}'' - \mathbf{r}_s)\mathrm{d}^2\mathbf{r}'\mathrm{d}^2\mathbf{r}'' + \exp(-i\phi) \\ & \int\int\int\int \tilde{M}(\mathbf{r}' - \mathbf{r}'')T(\mathbf{r}', t)T^*(\mathbf{r}'', t) \\ & \cdot \mathbf{E}^*_r(\mathbf{r}'' - \mathbf{r}_s) \cdot \mathbf{E}_o(\mathbf{r}' - \mathbf{r}_s)\mathrm{d}^2\mathbf{r}'\mathrm{d}^2\mathbf{r}''. \end{aligned}$$

We can simplify the notation here by writing

$$S(\mathbf{r}_s) \equiv B(\mathbf{r}_s) + \exp(i\phi)V(\mathbf{r}_s) + \exp(-i\phi)H(\mathbf{r}_s),$$

where B is the hologram bias, V encodes the virtual image, and H encodes the real image.[20]

Using heterodyne detection[11,21] or measurements at several values of the phase ϕ,[22] we can solve for the desired hologram H, with the bias and virtual image removed:

$$\begin{aligned} & H_2(\mathbf{r}_s) \\ & = \int\int\int\int \tilde{M}(\mathbf{r}' - \mathbf{r}'')T(\mathbf{r}', t)T^*(\mathbf{r}'', t)\mathbf{E}^*_r(\mathbf{r}'' - \mathbf{r}_s) \\ & \quad \cdot \mathbf{E}_o(\mathbf{r}' - \mathbf{r}_s)\mathrm{d}^2\mathbf{r}'\mathrm{d}^2\mathbf{r}'', \end{aligned} \quad (10)$$

where the subscript of H_2 denotes the double-beam scanning mode. We note here that because of the symmetry of $\mathbf{E}_o$ and $\mathbf{E}_r$ in Eq. (10), the distinction between reference and object beams is arbitrary.

A. Incoherent Mode

For the purely incoherent mode, we require that the signal generated by the detector be proportional to the sum over the intensity of the response of each point in the sample. To this end it is necessary to use a clear mask,[3] so that $M(\boldsymbol{\rho}) \cong 1$. In this case $\tilde{M}(\mathbf{r}) \cong \delta(\mathbf{r})$, and Eq. (10) becomes

$$\begin{aligned} H_{2,i}(\mathbf{r}_s) = {} & \int\int\int\int \delta(\mathbf{r}' - \mathbf{r}'')T(\mathbf{r}', t)T^*(\mathbf{r}'', t) \\ & \mathbf{E}^*_r(\mathbf{r}'' - \mathbf{r}_s) \cdot \mathbf{E}_o(\mathbf{r}' - \mathbf{r}_s)\mathrm{d}^2\mathbf{r}'\mathrm{d}^2\mathbf{r}'' \\ = {} & \int\int |T(\mathbf{r}', t)|^2\mathbf{E}^*_r(\mathbf{r}' - \mathbf{r}_s) \cdot \mathbf{E}_o(\mathbf{r}' \\ & - \mathbf{r}_s)\mathrm{d}^2\mathbf{r}' \\ = {} & |T(\mathbf{r}_s, t)|^2 \otimes [\mathbf{E}^*_r(\mathbf{r}_s) \cdot \mathbf{E}_o(\mathbf{r}_s)]. \end{aligned}$$

From Eq. (8) we see that for an arbitrary degree of coherence of the sample,

$$\begin{aligned} |T(\mathbf{r}_s, t)|^2 &= T_{\mathrm{ins}}(\mathbf{r})\exp[i\Psi(\mathbf{r}, t)]T^*_{\mathrm{ins}}(\mathbf{r})\exp[-i\Psi(\mathbf{r}, t)] \\ &= |T_{\mathrm{ins}}(\mathbf{r}_s)|^2, \end{aligned}$$

so that

$$H_{2,i}(\mathbf{r}_s) = |T(\mathbf{r}_s)|^2 \otimes [\mathbf{E}^*_r(\mathbf{r}_s) \cdot \mathbf{E}_o(\mathbf{r}_s)]. \quad (11)$$

We see that Eq. (11) has the same form as Eq. (1) and therefore represents the hologram of the intensity response $|T(\mathbf{r}_s)|^2$, with encoding function $\mathbf{E}^*_r(\mathbf{r}_s) \cdot \mathbf{E}_o(\mathbf{r}_s)$. Note that in general one can determine the encoding function by measuring the hologram of a point object, which then allows one to use Eq. (3) to estimate the appropriate reconstruction function.

If the reference beam is a uniform plane wave ($E_r \equiv 1$, constant polarization direction $\hat{\mathbf{E}}_r$), then to within a multiplicative constant Eq. (11) becomes

$$H_{2,i,\,pw}(\mathbf{r}_s) = |T(\mathbf{r}_s)|^2 \otimes [\hat{\mathbf{E}}_r \cdot \mathbf{E}_o(r_s)]. \quad (12)$$

If we make the assumption that the polarization direction of $\mathbf{E}_o(\mathbf{r}_s)$ is also constant, so that $\mathbf{E}_o(\mathbf{r}_s) = E_o(\mathbf{r}_s)\hat{\mathbf{E}}_o$, Eq. (12) reduces (to within a multiplicative constant) to

$$H_{2,i,\,pw,\mathrm{pol}}(\mathbf{r}_s) = |T(\mathbf{r}_s)|^2 \otimes E_o(\mathbf{r}_s). \quad (13)$$

This is of the same form as Eq. (21) of Indebetouw *et al.*[3] However, we now see that we require $\hat{\mathbf{E}}_o$ to be constant, as well as $\mathbf{E}_r$ to be a plane wave. Although in low-NA systems this is possible, in applications such as high-resolution microscopy, in which large-NA objective lenses are mandatory, the direction of polarization will vary with spatial position. In such cases, Eq. (12) must be used in place of Eq. (13). As Eq. (3) indicates, this will have an effect on the choice of the optimal reconstruction function to be used, because the encoding functions in Eqs. (12) and (13) are not the same.

B. Coherent Mode

For the coherent mode, we require that the detector signal be proportional to the squared modulus of the amplitude sum of the response of each point in the sample (which, of course, must emit coherently). We therefore restrict detection to a single point in Fourier space, so that the mask is a pinhole,[3] and $M(\boldsymbol{\rho}) = \delta(\boldsymbol{\rho} - \boldsymbol{\rho}_d)$, where $\boldsymbol{\rho}_d$ is the position of the pinhole. The FT of this is $\tilde{M}(\mathbf{r}) = \exp(-2\pi i\boldsymbol{\rho}_d \cdot \mathbf{r})$, so the hologram described by Eq. (10) becomes

$$\begin{aligned} H_{2,c}(\mathbf{r}_s) = {} & \int\int\int\int \exp(-2\pi i\boldsymbol{\rho}_d \\ & \cdot (\mathbf{r}' - \mathbf{r}''))T(\mathbf{r}')T^*(\mathbf{r}'')\mathbf{E}^*_r(\mathbf{r}'' - \mathbf{r}_s) \\ & \cdot \mathbf{E}_o(\mathbf{r}' - \mathbf{r}_s)\mathrm{d}^2\mathbf{r}'\mathrm{d}^2\mathbf{r}'' \\ = {} & \int\int \exp(2\pi i\boldsymbol{\rho}_d \cdot \mathbf{r}'')T^*(\mathbf{r}'')\mathbf{E}^*_r(\mathbf{r}'' - \mathbf{r}_s)\mathrm{d}^2\mathbf{r}'' \\ & \cdot \int\int \exp(-2\pi i\boldsymbol{\rho}_d \cdot \mathbf{r}')T(\mathbf{r}')\mathbf{E}_o(\mathbf{r}' - \mathbf{r}_s)\mathrm{d}^2\mathbf{r}' \\ = {} & \{[\exp(2\pi i\boldsymbol{\rho}_d \cdot \mathbf{r}_s)T^*(\mathbf{r}_s)] \bar{\otimes} \mathbf{E}^*_r(\mathbf{r}_s)\} \\ & \cdot \{[\exp(-2\pi i\boldsymbol{\rho}_d \cdot \mathbf{r}_s)T(\mathbf{r}_s)] \bar{\otimes} \mathbf{E}_o(\mathbf{r}_s)\}, \end{aligned} \quad (14)$$

where, using notation similar to that of Sheppard,[19] $\bar{\otimes}$ denotes the correlation of a scalar and a vector. Note that we have used the fact that for a coherent response, $T(\mathbf{r}, t) = T(\mathbf{r})$. Unfortunately, the "hologram" described by Eq. (14) is not of the basic form of Eq. (1) and is not useful for image reconstruction via a correlation, as described by Eq. (2).

However, if we again take the specific case in which the reference beam is a uniform plane wave, $H_{2,c}(\mathbf{r}_s)$ reduces to

$$H_{2,c,pw}(\mathbf{r}_s) = \mathbf{H}_{c0} \cdot \int\int \exp(-2\pi i \boldsymbol{\rho}_d \cdot \mathbf{r}') T(\mathbf{r}') \mathbf{E}_o(\mathbf{r}' - \mathbf{r}_s) \mathrm{d}^2\mathbf{r}'$$
$$= [\exp(-2\pi i \boldsymbol{\rho}_d \cdot \mathbf{r}_s) T(\mathbf{r}_s)] \otimes [\mathbf{H}_{c0} \cdot \mathbf{E}_o(\mathbf{r}_s)], \quad (15)$$

where $\mathbf{H}_{c0}$ is a constant. If we also assume that the mask is centered on the optical axis (i.e., $\rho_d = 0$), Eq. (15) reduces further to

$$H_{2,c,pw}(\mathbf{r}_s) = T(\mathbf{r}_s) \otimes [\mathbf{H}_{c0} \cdot \mathbf{E}_o(\mathbf{r}_s)]. \quad (16)$$

Equations (15) and (16) have the same form as Eq. (1), and the resulting hologram is linear in the amplitude response of the sample. Equation (16) is equivalent to Eq. (20) of Indebetouw *et al.*,[3] except that the high-NA polarization effects discussed in reference to incoherent OSH also apply here. However, this result is obtained only when the reference beam is an ideal, uniform plane wave. If this is not the case in practice, the disparity between the forms of Eqs. (1) and (14) shows that accurate reconstruction of the sample via Eq. (2) is not possible. This situation differs from the incoherent case, in which nonconstant $\mathbf{E}_r$ affects only the encoding function rather than the actual form of the resulting hologram. Since one of the important advantages of digital holography is that distortions due to known aberrations in the beams can be removed in the reconstruction,[23] the inability of double-beam coherent OSH to account for reference-beam aberrations can represent a significant drawback.

4. SINGLE-BEAM SCANNING

In the case of single-beam scanning, only the object beam is scanned (see Fig. 3). $\mathbf{E}_{\mathrm{ill}}$ is now

$$\mathbf{E}_{\mathrm{ill}}(\mathbf{r}, \mathbf{r}_s) = \mathbf{E}_o(\mathbf{r} - \mathbf{r}_s) + \exp(i\phi)\mathbf{E}_r(\mathbf{r}). \quad (17)$$

Equation (17) is identical to Eq. (6), except that $\mathbf{E}_r$ depends only on $\mathbf{r}$ instead of on $\mathbf{r} - \mathbf{r}_s$. Regarding nomenclature, the terms "object" and "reference" beam are no longer arbitrary: the reference beam now refers specifically to the beam that is not scanned.

It should therefore be clear that for illumination described by Eq. (17) instead of by Eq. (6), the hologram described by Eq. (10) becomes

$$H_1(\mathbf{r}_s) = \int\int\int\int \tilde{M}(\mathbf{r}' - \mathbf{r}'') T(\mathbf{r}', t) T^*(\mathbf{r}'', t) \mathbf{E}_r^*(\mathbf{r}'') \cdot \mathbf{E}_o(\mathbf{r}' - \mathbf{r}_s) \mathrm{d}^2\mathbf{r}' \mathrm{d}^2\mathbf{r}'', \quad (18)$$

where the subscript of H_1 denotes single-beam scanning. The only difference between Eqs. (18) and (10) is the change from $\mathbf{E}_r^*(\mathbf{r}'' - \mathbf{r}_s)$ to $\mathbf{E}_r^*(\mathbf{r}'')$, reflecting the fact that the reference beam is not scanned.

A. Incoherent Mode

As was the case for double-beam scanning, for the incoherent mode we again have $M(\boldsymbol{\rho}) \cong 1$ and $\tilde{M}(\mathbf{r}) \cong \delta(\mathbf{r})$, so Eq. (18) becomes

$$H_{1,i}(\mathbf{r}_s) = \int\int |T(\mathbf{r}', t)|^2 \mathbf{E}_r^*(\mathbf{r}') \cdot \mathbf{E}_o(\mathbf{r}' - \mathbf{r}_s) \mathrm{d}^2\mathbf{r}'$$
$$= (|T(\mathbf{r}_s)|^2 \mathbf{E}_r^*(\mathbf{r}_s)) \dot{\otimes} \mathbf{E}_o(\mathbf{r}_s), \quad (19)$$

where, as in Ref. 19, $\dot{\otimes}$ denotes the scalar correlation of two vector functions. As in the incoherent double-beam scanning case, the time dependence of $T(\mathbf{r}, t)$ disappears when we take the magnitude. Because of the vector nature of the correlation arguments in Eq. (19), the form is not the same as that of Eq. (1). Even if we know $H_{1,i}(\mathbf{r}_s)$ and $\mathbf{E}_o(\mathbf{r}_s)$, it is not possible to invert Eq. (19) to recover $|T(\mathbf{r}_s)|^2 \mathbf{E}_r^*(\mathbf{r}_s)$ and thus extract the desired information about the sample, $|T(\mathbf{r}_s)|^2$.

However, if the optics are designed so that the polarization of the reference beam is not a function of position (possible only in low-NA systems), i.e., $\mathbf{E}_r^*(\mathbf{r}_s) = E_r^*(\mathbf{r}_s)\hat{\mathbf{E}}_r$, then Eq. (19) becomes

$$H_{1,i,\mathrm{pol}}(\mathbf{r}_s) = (|T(\mathbf{r}_s)|^2 E_r^*(\mathbf{r}_s)) \otimes [\hat{\mathbf{E}}_r \cdot \mathbf{E}_o(\mathbf{r}_s)]. \quad (20)$$

Equation (20) now matches the form of Eq. (1) and describes the hologram of $|T(\mathbf{r}_s)|^2 E_r^*(\mathbf{r}_s)$. If $E_r^*(\mathbf{r}_s)$ is known, we can simply divide the image reconstructed from the hologram given by Eq. (20) by $E_r^*(\mathbf{r}_s)$ to obtain the intensity response $|T(\mathbf{r}_s)|^2$. Of course, we are still restricted to $E_r^*(\mathbf{r}_s) \neq 0$ for all $\mathbf{r}_s$ to ensure that $|T(\mathbf{r}_s)|^2$ is well defined over the entire field of view.

For this technique to be useful, we need to know $E_r^*(\mathbf{r}_s)$. However, this can be determined by measuring a calibration hologram with a uniform sample present. That is, with $T(\mathbf{r}_s) \equiv 1$ we measure

$$H_{1,i,cal}(\mathbf{r}_s) = E_r^*(\mathbf{r}_s) \otimes [\hat{\mathbf{E}}_r \cdot \mathbf{E}_o(\mathbf{r}_s)].$$

The image reconstructed from $H_{1,i,\mathrm{cal}}(\mathbf{r}_s)$ yields an estimate for $E_r^*(\mathbf{r}_s)$, which allows us to recover the undistorted image of the sample [i.e., $|T(\mathbf{r}_s)|^2$].

Of course, if we can arrange for the reference beam to be a uniform plane wave, Eq. (20) reduces to

$$H_{1,i,pw,\mathrm{pol}}(\mathbf{r}_s) = |T(\mathbf{r}_s)|^2 \otimes [\hat{\mathbf{E}}_r \cdot \mathbf{E}_o(\mathbf{r}_s)].$$

This represents a hologram linear in the intensity response, and there is no need for the calibration step described in the previous paragraph.

B. Coherent Mode

As with double-beam scanning, the mask for the coherent mode is a pinhole, $M(\boldsymbol{\rho}) = \delta(\boldsymbol{\rho} - \boldsymbol{\rho}_d)$, so that Eq. (18) becomes

$$H_{1,c}(\mathbf{r}_s)$$

$$= \int\int\int\int \exp(-2\pi i \boldsymbol{\rho}_d \cdot (\mathbf{r}' - \mathbf{r}''))T(\mathbf{r}')T^*(\mathbf{r}'')\mathbf{E}_r^*(\mathbf{r}'') \cdot \mathbf{E}_o(\mathbf{r}' - \mathbf{r}_s)\mathrm{d}^2\mathbf{r}'\mathrm{d}^2\mathbf{r}''$$

$$= \mathbf{H}_{c0} \cdot \int\int \exp(-2\pi i \boldsymbol{\rho}_d \cdot \mathbf{r}')T(\mathbf{r}')\mathbf{E}_o(\mathbf{r}' - \mathbf{r}_s)\mathrm{d}^2\mathbf{r}'$$

$$= [\exp(-2\pi i \boldsymbol{\rho}_d \cdot \mathbf{r}_s)T(\mathbf{r}_s)] \otimes [\mathbf{H}_{c0} \cdot \mathbf{E}_o(\mathbf{r}_s)], \quad (21)$$

where $\mathbf{H}_{c0} = \int\int \exp(2\pi i \boldsymbol{\rho}_d \cdot \mathbf{r}'')T^*(\mathbf{r}'')\mathbf{E}_r^*(\mathbf{r}'')\mathrm{d}^2\mathbf{r}''$ is a constant. As with coherent double-beam scanning, we have made use of the relationship $T(\mathbf{r}, t) = T(\mathbf{r})$ for a coherent sample response.

Here we have the desired coherent hologram of the sample: Except for the $\exp(2\pi i \boldsymbol{\rho}_d \cdot \mathbf{r}_s)$ factor, it is linear in $T(\mathbf{r}_s)$. Note that for the single-beam scanning method to get a useful coherent hologram of the sample, it is necessary neither for the reference beam to be a uniform plane wave nor for its polarization direction to be constant.

If we are again careful to align the detector on axis, so that $\rho_d = 0$ (as in Ref. 3), Eq. (21) becomes

$$H_{1,c}(\mathbf{r}_s) = T(\mathbf{r}_s) \otimes [\mathbf{H}_{c0} \cdot \mathbf{E}_o(\mathbf{r}_s)], \quad (22)$$

and the hologram of the sample is linear in the amplitude response of the sample. Note that the single-beam scanning coherent hologram [Eq. (22)] is the same as the double-beam scanning coherent hologram [Eq. (16)], although we did not need to make the plane-wave assumption for the reference beam.

Alternatively, if we accept that misalignments may occur (i.e., $\rho_d \neq 0$), we can measure a calibration hologram with a uniform sample [i.e., $T(\mathbf{r}_s) \equiv 1$]. From Eq. (21), the result would be

$$H_{1,c,\mathrm{cal}}(\mathbf{r}_s) = \exp(-2\pi i \boldsymbol{\rho}_d \cdot \mathbf{r}_s) \otimes [\mathbf{H}_{c0} \cdot \mathbf{E}_o(\mathbf{r}_s)].$$

The image reconstructed from this $H_{1,c,\mathrm{cal}}$ is simply $\exp(-2\pi i \boldsymbol{\rho}_d \cdot \mathbf{r}_s)$, which can be used to correct the image reconstructed from $H_{1,c}$ [given by Eq. (21)] for the $\rho_d \neq 0$ factor and obtain the desired image of the sample, $T(\mathbf{r}_s)$. Note that this calibration could also be used to correct the same problem in double-beam scanning [i.e., to account for the $\exp(-2\pi i \boldsymbol{\rho}_d \cdot \mathbf{r}_s)$ term in Eq. (15)]. Also, this calibration is mathematically equivalent to that described in Subsection 4.A for incoherent single-beam scanning, although the factor corrected for is $\exp(-2\pi i \boldsymbol{\rho}_d \cdot \mathbf{r}_s)$ instead of $E_r^*(\mathbf{r}_s)$.

5. THICK-SAMPLE CONSIDERATIONS

A. Condition for Sample Thinness

In Section 3 we required the sample to be thin. This is because for a thick sample, light is diffracted and/or absorbed as it passes through the sample [Fig. 4(a)]. Since the sample itself is responsible for this, the illumination pattern at any point inside (or behind) the sample becomes a function of the sample properties and position. The dependence of the illumination pattern on the scanner position is no longer simply translational, and Eqs. (6) and (17) must be rewritten as

$$\mathbf{E}_{\mathrm{ill}}(\mathbf{r}, \mathbf{r}_s) = \mathbf{E}_o(\mathbf{r}, \mathbf{r}_s) + \exp(i\phi) \cdot \mathbf{E}_r(\mathbf{r}, \mathbf{r}_s).$$

The scanned pattern is no longer translationally invariant, which means that such a system does not result in a hologram of the form of Eq. (1). (We have assumed a transmissive geometry here for illustrative purposes. However, in a reflecting configuration, the thin-sample restriction is still important to avoid multiple reflections, which would result in the same type of dependence of the scanned pattern on the sample position.)

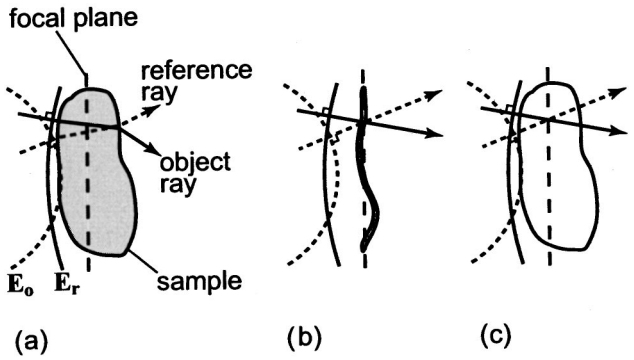

Fig. 4. Sample thickness effects. (a) In a thick sample, the light is refracted and/or absorbed as it passes through the sample. For points at some depth into the sample, the illumination pattern is dependent on the properties of the sample itself. (b) For a thin sample this is not a problem, because the illumination is not significantly altered before it exits the sample. (c) For a nonscattering fluorescent sample (as discussed in Subsection 5.B), the illumination pattern is not significantly affected by the sample, even when the sample is thick.

However, if the sample is sufficiently thin [Fig. 4(b)], we can define the effective two-dimensional response of the sample as

$$T(\mathbf{r}) = \int \frac{\delta T(\mathbf{r}, z)}{\delta z}\mathrm{d}z, \quad (23)$$

where the integral is over the sample thickness. We note that to make use of Eq. (23), the sample is required to be *thin*, but not necessarily *flat*, which emphasizes the advantage of making a holographic (i.e., 3D) recording.

We also note that this requirement of thinness is not restricted to OSH: It simply implies that with an aberrating sample, ideal image reconstruction is generally not possible. This is true not only of OSH but also of most other microscopy modes, such as confocal or wide-field fluorescence imaging (see Kam *et al.*[24] for a recent treatment of this issue).

B. Fluorescence Holography

Another possibility for the use of OSH with a thick sample is the special case of a sample that does not alter the illumination pattern to a significant extent and whose response is isotropic. An example of relevance to biological microscopy would be a fluorescent sample embedded in a suitable index-matched medium. If absorption is also negligible, the illumination pattern is essentially unaltered by the presence of the sample [see Fig. 4(c)]. If we restrict ourselves to incoherent imaging, for which

$M(\mathbf{r}) = 1$, the analysis of the imaging process can be greatly simplified over that presented in Section 2, and it can be shown that OSH is compatible with 3D fluorescent samples. (The technique has already been demonstrated experimentally and described with the use of objective-lens-less OSH.[10,25] We present the following analysis to account explicitly for the 3D nature of the sample and to place it in context with the descriptions in Section 2.)

Consider the case of double-beam scanning: As in Subsection 2.A, the illumination is described by Eq. (6), which we now rewrite to include the axial position explicitly:

$$\mathbf{E}_{\text{ill}}(\mathbf{r},\ \mathbf{r}_s\,,\ z) = \mathbf{E}_o(\mathbf{r} - \mathbf{r}_s\,,\ z) + \exp(i\phi)\mathbf{E}_r(\mathbf{r} - \mathbf{r}_s\,,\ z). \tag{24}$$

Note that if we did not include the nonscattering, nonrefracting, weakly absorbing conditions, scanning the beams would not simply translate the interference pattern. Equation (24) would then have to be rewritten as

$$\mathbf{E}_{\text{ill}}(\mathbf{r},\ \mathbf{r}_s\,,\ z) = \mathbf{E}_o(\mathbf{r},\ \mathbf{r}_s\,,\ z) + \exp(i\phi)\mathbf{E}_r(\mathbf{r},\ \mathbf{r}_s\,,\ z).$$

The difference appears minor here, but it is crucial to the linearity that allows the OSH holograms to have the form of correlations, as in Eq. (1).

The fluorescence intensity response to the excitation given by Eq. (24) is described (to within a multiplicative constant) by

$$I_{\text{em}}(\mathbf{r},\ \mathbf{r}_s\,,\ z) = T_{\text{fl}}(\mathbf{r},\ z)|\mathbf{E}_{\text{ill}}(\mathbf{r},\ \mathbf{r}_s\,,\ z)|^2,$$

where $T_{\text{fl}}(\mathbf{r},\ z)$ is the spatial distribution of the fluorophore. To be comprehensive, one should account for the fact that both the excitation and the emission probabilities for a fluorophore are (spatially) nonisotropic, and therefore the polarization of the illumination will have an effect. For the vast majority of fluorescence microscopy applications, the dye molecules are rotationally free to diffuse on typical measurement time scales. This means that the anisotropies are averaged out, and the detected signal is independent of the illumination polarization. Although there are some cases—particularly when the fluorophores are rigidly embedded in and, in terms of their orientation, correlated with, an anisotropic matrix—when polarization effects may become manifest, these represent a minority of cases and are not considered here.

With the assumptions that the fluorescent emission is isotropic (i.e., the dipole rotational diffusion time is short compared with the detector integration time) and that the optical system is arranged so as to avoid vignetting of the sample, it should be clear that in the absence of a mask, the signal at the large-area detector (see Fig. 2) is proportional to the total fluorescence emitted by the sample:

$$\begin{aligned} S(\mathbf{r}_s) &= \int\int\int I_{\text{em}}(\mathbf{r},\ \mathbf{r}_s\,,\ z)\mathrm{d}^2\mathbf{r}\mathrm{d}z \\ &= \int\int\int |T_{\text{fl}}(\mathbf{r},\ z)|^2[|\mathbf{E}_o(\mathbf{r} - \mathbf{r}_s\,,\ z)|^2 \\ &\quad + |\mathbf{E}_r(\mathbf{r} - \mathbf{r}_s\,,\ z)|^2 \\ &\quad + \exp(i\phi)\mathbf{E}_r(\mathbf{r} - \mathbf{r}_s\,,\ z)\mathbf{E}_o^*(\mathbf{r} - \mathbf{r}_s\,,\ z) \\ &\quad + \exp(-i\phi)\mathbf{E}_r^*(\mathbf{r} - \mathbf{r}_s\,,\ z)\mathbf{E}_o(\mathbf{r} - \mathbf{r}_s\,,\ z)]\mathrm{d}^2\mathbf{r}\mathrm{d}z, \end{aligned}$$

where the integral is over the sample volume. As in Section 3, heterodyne techniques can be used to eliminate the bias and virtual image portions of the hologram, so that we are left with

$$\begin{aligned} H_{\text{fl}}(\mathbf{r}_s) &= \int\int\int |T_{\text{fl}}(\mathbf{r},\ z)|^2\mathbf{E}_r^*(\mathbf{r} - \mathbf{r}_s\,,\ z) \\ &\quad \cdot \mathbf{E}_o(\mathbf{r} - \mathbf{r}_s\,,\ z)\mathrm{d}^2\mathbf{r}\mathrm{d}z \\ &= \int |T_{\text{fl}}(\mathbf{r}_s\,,\ z)|^2 \otimes [\mathbf{E}_r^*(\mathbf{r}_s\,,\ z) \cdot \mathbf{E}_o(\mathbf{r}_s\,,\ z)]\mathrm{d}z. \end{aligned} \tag{25}$$

The integrand of Eq. (25) now has the same form as Eq. (1), so the hologram of the thick fluorescent object is simply the sum of the contributions from each z plane. Any given plane in the sample can be reconstructed by selecting the reconstruction function for the appropriate depth, z [i.e., Eq. (3), with $R_f(\mathbf{r}) \approx \mathbf{E}_r^*(\mathbf{r},\ z) \cdot \mathbf{E}_o(\mathbf{r},\ z)$]. However, as the out-of-focus light from other depths is also included, this form of OSH does not provide optical sectioning.

The above derivation was performed for the double-beam scanning configuration. However, it is straightforward to show that an analogous result applies to single-beam scanning, with the same restrictions on the polarization of $\mathbf{E}_r$ as applied in Section 4.

6. DISCUSSION

Table 1 summarizes the results of the different scanning modes and lists the requirements for a useful hologram to be generated.

With *incoherent-mode* double-beam scanning OSH, a useful hologram is obtained without any special assumptions about the wave-front polarizations or curvatures or the NA of the system. If one assumes that the reference beam is a uniform plane wave and that the polarization direction of the object beam is constant, then the results presented here reduce to those of Indebetouw *et al.*[3]

Table 1. Summary of the Different OSH Modes

Mode	Double-Beam Scanning	Single-Beam Scanning
Incoherent	$H_{2,i}(\mathbf{r}_s) = \lvert T(\mathbf{r}_s)\rvert^2 \otimes [\mathbf{E}_r^*(\mathbf{r}_s) \cdot \mathbf{E}_o(\mathbf{r}_s)]$ general	$H_{1,i,\text{pol}}(\mathbf{r}_s) = (\lvert T(\mathbf{r}_s)\rvert^2 E_r^*(\mathbf{r}_s)) \otimes [\hat{\mathbf{E}}_r \cdot \mathbf{E}_o(\mathbf{r}_s)]$ requires constant polarization of reference beam
Coherent	$H_{2,c,\,pw}(\mathbf{r}_s) = T(\mathbf{r}_s) \otimes [\mathbf{H}_{c0} \cdot \mathbf{E}_o(\mathbf{r}_s)]$ requires uniform plane wave for reference beam	$H_{1,c}(\mathbf{r}_s) = T(\mathbf{r}_s) \otimes [\mathbf{H}_{c0} \cdot \mathbf{E}_o(\mathbf{r}_s)]$ general

There is no need to measure a calibration hologram to compensate for aberrations in the reference beam, as these are accounted for in the hologram encoding function.

In contrast, with *coherent-mode* double-beam scanning OSH, it is necessary to have a uniform plane wave as the reference beam if the resulting "hologram" is to be of use. Given this restriction, and that the polarization direction of the object beam is constant, our results again reproduce those of Indebetouw *et al.*[3] Although it is not necessary to calibrate for aberrations in the reference beam, if one cannot ensure that the pinhole mask is exactly on axis, it is necessary to measure a calibration hologram to remove the phase-modulation artifacts caused by this misalignment.

For single-beam scanning, to generate a useful *incoherent* OSH hologram, we require that the polarization of the reference beam be constant. In practice, if one intends to use one beam that is approximately collimated, this restriction is easily fulfilled. However, if one considers employing reference and object beams both with large wavefront curvature, then this issue may become significant. Also, in this case it is necessary to measure the hologram of a uniform sample to calibrate the reference beam if its characteristics are not known *a priori*.

In single-beam scanning, the *coherent* mode requires no special restrictions on the beam characteristics. As with the double-beam case, however, a calibration may be needed to account for misalignments of the detection pinhole.

In general, for the mathematical description discussed here to be accurate, the sample is required to be thin. This allows one to avoid the effects of refraction or multiple-scattering events of the illumination beam. An exception to this restriction is the case in which the sample does not alter the illumination field significantly and has a uniform response. Fluorescence microscopy of biological samples embedded in a suitably index-matched medium is an example of this exception. With such samples it is also generally desirable to be able to account for the effects of high-NA objective lenses, as is done in this paper.

7. CONCLUSIONS

We have generalized the model of OSH so that it can account for arbitrary illumination beams and high-NA optics. This allows us to relax the restriction that one of the interfering illumination beams must be a uniform plane wave and to model the effects of the polarization that must be included if OSH is to be implemented in high-resolution microscopy. The main motivation for this is the potential that we see in OSH for applications in biological microscopy. The ability to map three dimensionally both the specimen's refractive index and the emission of fluorescence labels is of great interest in the life science community.

We have also presented here the possibility of single-beam scanning OSH, and we compared the technique with double-beam scanning. The results suggest that although double-beam scanning appears well suited to incoherent OSH, the restriction of a uniform plane reference beam for coherent OSH may result in practical problems in aberrating systems. This is a significant drawback, because one of the advantages of digital holography in general is the ability to compensate for such aberrations. The single-beam scanning method outlined here eliminates this problem. Although single-beam scanning incoherent OSH does have the restriction of constant polarization direction of the reference beam, this restriction is generally easier to accommodate than that of the uniform plane wave for coherent double-beam scanning OSH. Therefore, if a single system capable of both coherent and incoherent OSH is desired, it would seem that single-beam scanning is the more robust solution.

Future work includes implementation of a high-NA OSH system, which is ideally capable of observation of live biological specimens in both fluorescence and phase contrasts. It also remains to be seen whether OSH as described here can be modified so as to be able to provide useful information about arbitrary 3D samples. This would indeed make OSH a powerful imaging technique for many applications.

ACKNOWLEDGMENTS

The authors thank Alexander Rohrbach for his careful and insightful comments on the manuscript during preparation. They also express their gratitude for the financial support of the following: the Bundesministerium für Bildung und Forschung (to J. Huisken, E. H. K. Stelzer, and J. Swoger); the Deutscher Akademischer Austauschdienst (to E. H. K. Stelzer and J. Swoger); and Plan Nacional I + D + I under grant DPI2000-0774, Ministerio de Ciencia y Tecnología, Spain (to M. Martínez-Corral). M. Martínez-Corral's stay at the European Molecular Biology Laboratory was financed by the Accion Integrada HA1999-0102, Ministerio de Ciencia y Tecnología, Spain.

During the preparation of the paper, M. Martínez-Corral was on leave from the Departamento de Óptica, Universidad de Valencia, Dr. Moliner 50, 46100 Burjassot, Spain.

Correspondence should be directed to Jim Swoger: phone, 49-6221-387122; fax, 49-6221-387306; e-mail, jim.swoger@embl-heidelberg.de.

REFERENCES

1. T.-C. Poon, K. B. Doh, B. W. Schilling, M. H. Wu, K. Shinoda, and Y. Suzuki, "Three-dimensional microscopy by optical scanning holography," Opt. Eng. **34**, 1338–1344 (1995).
2. E. Hecht, *Optics*, 2nd ed. (Addison-Wesley, Don Mills, Ontario, 1987), pp. 593–610.
3. G. Indebetouw, P. Klysubun, T. Kim, and T.-C. Poon, "Imaging properties of scanning holographic microscopy," J. Opt. Soc. Am. A **17**, 380–390 (2000).
4. J. White, L. Johannes, F. Mallard, A. Girod, S. Grill, S. Reinsch, P. Keller, B. Tzschaschel, A. Echard, B. Goud, and E. H. K. Stelzer, "Rab6 coordinates a novel golgi to ER retrograde transport pathway in live cells," J. Cell Biol. **147**, 743–759 (1999).
5. J. Lippincott-Schwartz, J. F. Presley, K. J. M. Zaal, K. Hirschberg, C. D. Miller, and J. Ellenberg, "Monitoring the dynamics and mobility of membrane proteins tagged with

green fluorescent protein," in *Methods in Cell Biology*, K. F. Sullivan and S. A. Kay, eds. (Academic, San Diego, 1999), Vol. 58, pp. 261–281.
6. R. F. VanLigten and H. Osterberg, "Holographic microscopy," Nature **211**, 282–283 (1966).
7. S. Schedin, G. Pedrini, and H. J. Tiziani, "Pulsed digital holography for deformation measurements on biological tissues," Appl. Opt. **39**, 2853–2857 (2000).
8. J. Jonkman and E. H. K. Stelzer, "Resolution and contrast in confocal and two-photon microscopy," in *Confocal and Two-photon Microscopy: Foundations, Applications, and Advances*, A. Diaspro, ed. (Wiley–Liss, New York, 2001), pp. 101–125.
9. T.-C. Poon, K. B. Doh, B. Schilling, K. Shinoda, Y. Suzuki, and M. H. Wu, "Holographic three-dimensional display using an electron-beam-addressed spatial light modulator," Opt. Rev. **4**, 567–571 (1997).
10. B. W. Schilling, T.-C. Poon, G. Indebetouw, B. Storrie, K. Shinoda, Y. Suzuki, and M. H. Wu, "Three-dimensional holographic fluorescence microscopy," Opt. Lett. **22**, 1506–1508 (1997).
11. T.-C. Poon, T. Kim, G. Indebetouw, B. W. Schilling, M. H. Wu, K. Shinoda, and Y. Suzuki, "Twin-image elimination experiments for three-dimensional images in optical scanning holography," Opt. Lett. **25**, 215–217 (2000).
12. T.-C. Poon, "Scanning holography and two-dimensional image processing by acousto-optic two-pupil synthesis," J. Opt. Soc. Am. A **2**, 521–527 (1985).
13. B. D. Duncan and T.-C. Poon, "Gaussian beam analysis of optical scanning holography," J. Opt. Soc. Am. A **9**, 229–236 (1992).
14. P. Klysubun and G. Indebetouw, "*A posteriori* processing of spatiotemporal digital microholograms," J. Opt. Soc. Am. A **18**, 326–331 (2001).
15. P. J. Shaw, "Comparison of wide-field/deconvolution and confocal microscopy for 3D imaging," in *Handbook of Biological Confocal Microscopy*, 2nd ed. J. B. Pawley, ed. (Plenum, New York, 1995), pp. 373–387.
16. L. O. Heflinger, R. F. Wuerker, and R. E. Brooks, "Holographic interferometry," J. Appl. Phys. **37**, 642–649 (1966).
17. S.-G. Kim, B. Lee, and E.-S. Kim, "Removal of bias and the conjugate image in incoherent on-axis triangular holography and real-time reconstruction of the complex hologram," Appl. Opt. **36**, 4784–4791 (1997).
18. Y. Takaki and H. Ohzu, "Fast numerical reconstruction technique for high-resolution hybrid holographic microscopy," Appl. Opt. **38**, 2204–2211 (1999).
19. C. J. R. Sheppard, "Vectors and Fourier transforms in optics," Optik **110**, 157–160 (1999).
20. Y. Takaki, H. Kawai, and H. Ohzu, "Hybrid holographic microscopy free of conjugate and zero-order images," Appl. Opt. **38**, 4990–4996 (1999).
21. F. Le Clerc, L. Collot, and M. Gross, "Numerical heterodyne holography with two-dimensional photodetector arrays," Opt. Lett. **25**, 716–718 (2000).
22. I. Yamaguchi and T. Zhang, "Phase-shifting digital holography," Opt. Lett. **22**, 1268–1270 (1997).
23. A. Stadelmaier and J. H. Massig, "Compensation of lens aberrations in digital holography," Opt. Lett. **25**, 1630–1632 (2000).
24. Z. Kam, B. Hanser, M. G. L. Gustafsson, D. A. Agard, and J. W. Sedat, "Computational adaptive optics for live three-dimensional biological imaging," Proc. Natl. Acad. Sci. USA **98**, 3790–3795 (2001).
25. G. Indebetouw, T. Kim, T.-C. Poon, and B. W. Schilling, "Three-dimensional location of fluorescent inhomogeneities in turbid media by scanning heterodyne holography," Opt. Lett. **23**, 135–137 (1998).